Discrepancies in the Prediction of Solar Wind using Potential Field Source Surface Model: An Investigation of Possible Sources

Bala Poduval and Xue Pu Zhao
Hansen Experimental Physics Laboratory
Stanford University, Palo Alto, CA 94305

April 29, 2004

Abstract

An inverse correlation has been found to exist between the magnetic flux tube expansion factor (FTE) at the source surface and the solar wind speed observed at Earth, which has been made use of in the prediction of solar wind speed near the Earth with reasonable accuracy. However, the correlation between FTE and the observed solar wind speed at Earth is not consistently high always and the discrepancies between the observed and predicted solar wind speed are quite significant. There are several factors causing this discrepancy. The present work is an investigation of such factors and an estimation of error caused by them. We found that one of the free parameters of the model, the number of multipole components included in the spherical harmonic expansion in the PFSS model, N_{max}, has tremendous influence on the location of photospheric foot points of coronal features as well as the computation of FTE. Another important factor is the transit time of solar wind used in the inverse mapping. Approximate values of this parameter that are currently being used can lead to significant errors in the predicted solar wind speed. We also present a detailed discussion on the importance of considering interaction between slow and fast solar wind streams in the inverse mapping technique.

1 Introduction

The relation between magnetic flux tube expansion near the Sun and the solar wind speed observed at earth was first noted by Levine, Altschuler and Harvey (Levine et al., 1977). They found that the fastest solar wind stream correlated with the least expanding magnetic flux tubes. Wang and Sheeley (1990) revisited this aspect and obtained an inverse relation between flux tube expansion factor (FTE) and solar wind speed (SWS) observed near Earth. This inverse relation has been made use of in the prediction of solar wind speed at 1 AU using a potential field source surface (PFSS) model of the corona (Arge and Pizzo, 2000). The predicted solar wind speed was found to agree fairly well with the observed speed near the Earth. However, there were significant discrepancies as pointed out by several authors (Bala, 2000, for instance). The limitation of the measurement of global photospheric magnetic field, inadequacy of the inverse mapping and the limitation of the PFSS model itself are a few factors contributing to the discrepancy. Arge and Pizzo (2000) have applied various corrections to the synoptic maps of photospheric fields which resulted in better overall agreement between the prediction and observation. However, discrepancies still exist.

Determination of the relation between FTE and SWS involves two steps. The first one is the identification of the precise location of solar wind source in the corona. For this, a technique called inverse mapping is usually employed. That is, the observed solar wind is traced back to the corona along the Archimedian spiral assuming little radial acceleration (constant speed) and pure radial flow, neglecting interaction between fast and slow solar wind streams, using the equation:

$$\begin{aligned} \phi_{ss} &= \phi_E + \frac{R\omega}{V} \\ \theta_{ss} &= \theta_E \end{aligned} \tag{1}$$

where, θ_{ss}, ϕ_{ss} and θ_E, ϕ_E are the heliographic latitudes and Carrington longitudes of a point at the source surface and at distance R from the Sun, respectively; ω, the angular speed of solar rotation and V, the solar wind speed. It is customary to use an approximate value for V, *constant speed approximation*, corresponding to an average solar wind transit time, irrespective of the observed daily values. Different authors use different transit times 4, 4.5 or 5 days or 27-day running average (e.g., Crooker et al., 1997; Wang et al., 1997; Wang and Sheeley, 1990). Since all other parameters in Eq. 1 are constants, the Carrington longitude of the source point of solar wind on the source surface is entirely determined by V.

The second step involves the calculation of FTE at location (θ_{ss} and ϕ_{ss}) on the source surface determined in Step 1. Since coronal magnetic field measurements are still not possible globally, one has to resort to coronal models such as PFSS. The FTE can be represented mathematically as:

$$FTE = \left(\frac{R_\odot}{R_{ss}}\right)^2 \frac{B_r(\theta_\odot, \phi_\odot)}{B_r(\theta_{ss}, \phi_{ss})} \tag{2}$$

where, $B_r(\theta_{ss}, \phi_{ss})$ denotes the magnetic field strength at location (θ_{ss} and ϕ_{ss}) on the source surface and $B_r(\theta_\odot, \phi_\odot)$ is the field strength at the photospheric footpoint of the flux tube traversing (θ_{ss} and ϕ_{ss}). $R_\odot$ and R_{ss} are the photospheric and source surface radii, respectively. To obtain $\mathrm{B}_r(\theta_\odot, \phi_\odot)$ the field at (θ_{ss}, ϕ_{ss}) has to be traced to photosphere along the magnetic field line. This procedure can be influenced by the free parameters of the model such as the truncation (N_{max}) of the spherical harmonic expansion or the source surface radius. Therefore, the accuracy of the predicted solar wind speed depends on the precision of the above two steps.

The present paper focuses on the influence of solar wind speed, V, on the inverse mapping and N_{max} on the computation of FTE. The paper presents a discussion of the importance of choosing the right values for these parameters as well as the importance of taking into account the interaction between fast and slow winds in the inverse mapping.

2 Truncation of spherical harmonic expansion

In this paper, we used the potential field source surface model with radial boundary condition. Hoeksema (1984) has shown that a source surface height of 2.5 $R_\odot$ produces results that are in better agreement with observations of current sheet crossings. Therefore, we used the same height in this paper. The value of N_{max} depends on the spatial resolution of the photospheric field maps. That is, the higher the resolution, the larger the value of N_{max}. For example, the Wilcox Solar Observatory (WSO) has a spatial resolaution of $5^\circ \times 5^\circ$ in latitude and longitude, whereas the National Solar Observatory at Kitt Peak (KPNO) has a spatial resolution of $1^\circ \times 1^\circ$. That is, it is possible to use $N_{max} = 90$ for the KPNO data, but certainly not for the WSO data. And, a larger value of N_{max} in turn will give a higher value of the FTE computed (Wang, 2004; Hakamada and Kojima, 1999). In our calculation the spatial resolution of KPNO has been lowered to that of WSO, for the sake of consistency. It is very common to use $N_{max} = 9$ for computing the source surface fields and N = 17, 23, 31, ... to determine foot points by tracing field lines or to compute expansion factors. Wang and Sheeley used $N_{max} = 17$ in one of the calculations (Wang and Sheeley, 1992; here they used WSO data) and $N_{max} = 31$ in subsequent studies (e. g., Wang and Sheeley, 1994, using WSO data). Hakamada, Kojima and their coworkers used $N_{max} = 90$ in their works (Hakamada and Kojima, 1999; Hakamada et al., 2002) using the Kitt Peak data. We have investigated the effect of N_{max}, for a given set of photospheric field data, e. g., WSO, on the photospheric foot points of coronal features, $(\theta_\odot, \phi_\odot)$ as well as on the computed values of FTE. For the present study, we used photospheric magnetic field data for CR 1829.

2.1 Variation in $\theta_\odot$ and $\phi_\odot$ with N_{max}

We computed the foot points $(\theta_\odot, \phi_\odot)$ of open field lines at a number of locations on the source surface (θ_{ss}, ϕ_{ss}), using N_{max} from 9 to 32. Taking $N_{max} = 9$ as reference, we obtained the differences $\delta\theta$ and $\delta\phi$ in $\theta_\odot$ and $\phi_\odot$, respectively, for each

N_{max} and plotted in Figures 1 and 2. We found that, on average, $\delta\theta$ and $\delta\phi$ varied within $\pm 2^\circ$. Only variations larger than this are depicted in Figures 1 and 2; hence the randomness in the values (θ_{ss}, ϕ_{ss}). On each panel, 'wso' stands for Wilcox Solar Observatory, the photospheric magnetic field data used and the numbers in parenthesis represent the location, in heliographic coordinates, of open field lines on the source surface (θ_{ss}, ϕ_{ss}) whose photospheric footpoints are obtained. The vertical line corresponds to $N_{max} = 22$.

The deviations do not show any latitudinal or longitudinal dependence. They are different at different locations and show random fluctuations rather than a systematic variation with N_{max}. Note that the largest deviation is between $N_{max} = 9$ and $N_{max} = 10$, 11 or 12, in most cases. Locations (45, 310) and (15, 170) showed deviations $> 10^\circ$. Here, $\delta\theta$ are $\sim 20^\circ$ and 15°, respectively, and $\delta\phi$, 12° and 60°, respectively. The deviations are less fluctuating above $N_{max} = 22$ and is nearly constant for most locations.

This excercise shows the influence of one of the free parameters, N_{max}, in the model on the determination of photospheric foot points of coronal features using PFSS model. The error or uncertainty in the photospheric foot points of a feature on source surface when traced back along the magnetic field lines can be as high as 60° in longitude and 20° in latitude. The open field lines on the source surface come from a maximum of 25% of the photospheric area during sunspot minimum and a minimum of 5% during sunspot maximum (Fig. 6 in Wang and Sheeley, 1992; Fig. 3 in Wang and Sheeley, 2002). Since the photospheric foot points of coronal open field lines are confined to such a narrow area, we believe that, the fluctuations of magnitude presented here could lead to a "wrong" source. That is, an event on the source surface will be traced to a region on the photosphere which may not be causally connected to the event at all. This could possibly explain why the source of solar wind has been identified as active regions in certain studies.

2.2 Variation of FTE with N_{max}

Figure 3 shows the variation of FTE with N_{max} at locations depicted in Figures 1 and 2. The vertical dashed line correspond to $N_{max} = 22$. Here, the source surface locations look randomly selected. This is because we present only those locations where $\delta\theta$ and $\delta\phi$ are greater than $\pm 2^\circ$, as mentioned in the previous section.

In general, instead of a tendency to converge with increasing N_{max}, FTE shows large fluctuations, especially below $N_{max} = 22$. According to Wang and Sheeley FTE > 20 imply sources of slow solar wind, i.e, speed ≤ 450 km s^{-1} (Wang and Sheeley, 1990; 1994; Wang et al., 1997). Therefore, fluctuations in FTE above this range affects the prediction of finer details of the slow solar wind. That is, even though the precise value of a particular solar wind stream may alter, the sources are still that of slow wind. This is the case at location (60, 260) and partially (below $N_{max} = 22$) at (45, 310) in Figure 3. In all other cases, FTE varies between 0 and 20, in general. Such a variation implies that depending on N_{max} used in the model, the speed of solar wind emanating from a given point (θ_{ss}, ϕ_{ss}) on the source

surface can be anywhere between 300 and 900 km s^{-1}!! This in turn implies that the prediction of solar wind speed based on PFSS model becomes "unpredictable", or highly dependent on one of the free parameters in the model.

From Figures 1–3, we see that the effect of N_{max} on $\theta_\odot, \phi_\odot$ and thereby on FTE is rather insignificant above $N_{max} = 22$. Therefore, $N_{max} = 22$ can safely be selected as an optimum value for all computations. However, to illustrate this point further, we reconstructed the photospheric field using different N_{max} in PFSS model. The first panel on the left in Figures 4 and 5 depict the photospheric magnetic field, for CR 1763, observed at WSO and Kitt Peak, respectively. The remaining panels represent the reconstructed photospheric field using $N_{max} = 16$ to $N_{max} = 28$. We, then, obtained the correlation coefficient between the observed and computed fields. This has been done for 60 Carrington rotations, between 1985 and 1989, and the correlation coefficients are plotted in Figures 6 and 7. From these figures, it is clear that $N_{max} = 22$ gives the best results, though there are some exceptions. Therfore, in all subsequent calculations we used $N_{max} = 22$ as an optimum value.

3 Influence of Inverse Mapping on FTE and Solar Wind Source

As discussed in Section 1, determination of the correlation of interplanetary events with the photospheric features involves two steps: mapping the interplanetary event back to the corona and determination of its photospheric footpoint. The first step is carried out by using Eq. 1. In this, the solar wind speed, V, used by different authors are different. That is, a constant speed corresponding to a transit time of 5 days, 345 km s^{-1}, (Crooker et al., 1997) or 4.5 days (380 km s^{-1}) or 4 days (428 km s^{-1}). While studying the Ulysses data, Wang et al., (1997) have taken a 27–day running average of observed solar wind speed to map the daily averaged solar wind back to the source surface. And, the most appropriate method, apparently, will be to use daily values of the observed solar wind (Neugebauer et al., 2002). In the present study, we used all these values to map the solar wind back to the source surface, and the Carrington longitude of the source point is obtained using Eq. 1 and the Carrington rotation number. The latitude has been taken the same as the latitudinal location of the observed wind near Earth on each day, or b0 angle. Then, the FTE has been calculated at each of these points on the source surface, using $N_{max} = 22$.

3.1 Correlation between FTE and Solar Wind Speed at 1 AU

Figure 8 shows the correlation between SWS and $\log_{10}$(FTE) obtained for different phases of solar cycle using different transit times in the inverse mapping procedure. For a comparison, we obtained the correlation coefficient for the same periods of solar minima and maxima as that of Wang (1995): 1976–77, 1982–87 and 1992–96 and, 1978–81 and 1988–91, respectively. The correlation coefficient, averaged over

a few years, does not show large variation with different transit times in inverse mapping. This does not imply that the influence of transit time on inverse mapping of individual events is negligible, which will be addressed in the next section. It should be more accurate to take the daily observed values of solar wind for the inverse mapping and the constant transit time will only introduce larger errors.

Figures 9 and 10 show scatter plots between SWS and $\log_{10}$(FTE), for 1992–96, and 1982–1987, when the correlation coefficient obtained was the highest and the lowest, respectively. In these figures, the daily values of solar wind speed were used for inverse mapping. As seen from Figures 9 and 10, the solar wind tends to be faster corresponding to lower values of FTE on the source surface while slow solar wind emanates from regions of large FTE. However, it is to be emphasized that there is large scatter about this mean trend, as already pointed out by Wang in his paper (Wang, 1995). That is, places where the solar wind is predicted to be fast (slow) by PFSS model, slow (fast) wind is observed. In otherwords, the observation does not match with the prediction. The results of the investigation of this dispcrepancy will be discussed in detail, in another paper.

Referring to Figures 8, 9 and 10, we notice that correlation coefficient is different for different phases of solar activity, and is not consistently low or high, during the period of study. It is interesting to note that correlation coefficient during 1992–96 is larger than that during 1982–87 by about a factor of 1.5, though both the periods are declining phases. The physical significance, if any, of this behaviour is not yet clear.

3.2 Influence of Inverse mapping on Carrington longitude and FTE

The range in the heliographic longitude introduced by different inverse mapping techniques is depicted in Figure 11. When the daily values of observed solar wind are used, the longitudes on the solar surface are shifted in the range 25° – 75°. That is, the longitudes of slow (300 km s^{-1}) and fast (900 km s^{-1}) solar wind are separated by 50°, i. e., they are distinguishable. On the other hand, the shift when using a 27-day running average has a range between 45° and 50°. That is, all the observed solar wind are traced back to a region bounded within this range of longitude. An average transit time of 5 days (corresponding to a speed of 345 km s^{-1}) takes the solar wind to longitude 65°, while 4.5 and 4 days will take it to longitudes 59° and 52°, respectively. Therefore, we see that the difference in the location of the solar wind source determined using the daily values and different "constant transit times" is at least 10° and at the most 40°, or an average of 25°, depending on the actual value of the solar wind speed on that day. An uncertainty of this magnitude can cause significant differences in the computed FTE, especially near the HCS.

We have seen in Figure 8 that the correlation coefficient, obtained as an average over several years, is not drastically altered by the method chosen for the inverse mapping. However, it has tremendous influence on the precise location of solar wind source on the source surface and thereby on the values of FTE computed for each

day. The difference in longitude of the solar wind source obtained using different inverse mapping is depicted in Figure 12. The histograms are obtained for different phases of solar cycle. For calculating the shift, we took the longitude obtained using the daily values of solar wind speed in Eq. 1, as a reference value and the shifts are the deviations from this value when using other methods. We found that more than 50% of cases had shifts in longitude greater than 10°. Also, more than 20% of cases had a shift > 20° and about 5% of cases had a shift > 30° (32° – 42°). Note that all these values are significant enough to confuse the source of solar wind. Correspondingly, the FTE varies across the ranges defined by Wang and Sheeley. Prediction of solar wind speed using this FTE may result in large deviations from the observed values, leading to the failure of the prediction.

4 Conclusion and Discussion

In this paper, the focus is on the influence two parameters, the solar wind speed (V) used in the inverse mapping technique given by Eq. 1 and the number of mulipole components used in the spherical harmonic expansion of the photospheric field in the PFSS model, N_{max}, on the determination of the flux tube expansion factor (Eq. 2) that is used to predict the solar wind speed near the Earth. We have shown that the *constant speed approximation* in the inverse mapping technique (Eq. 1) is a very sensitive parameter in the determination of coronal sources of solar wind. The location identified as the source of solar wind can differ by 25° in longitude, on average, depending on the value of V used. Further, this difference, in turn, causes significant change in the computed values of flux tube expansion factor (FTE), which has been made use of in the prediction of solar wind speed near the Earth. These results suggest that the *constant speed approximation* is not very effective, since different "constant speeds", corresponding to different constant transit times (Section 3.), can lead to totally "wrong" sources of solar wind on the corona and the stream–stream interaction cannot be ignored in the inverse mapping. Also, the present study reveals that N_{max} has a determining influence on the identification of photospheric footpoints of open field lines on the source surface. We have shown that the locations obtained using different N_{max} for a given set up in the PFSS model differ treamendously from one another (as high as about 36° in longitude and 18° in latitude) and the FTE computed at these points are substantially different. The difference is so significant that the prediction using them can be completely misleading. Therefore, it is necessary to have a consistent set of rules for choosing these two governing parameters for the success of the FTE–SWS relation in predicting the solar wind at 1 AU.

The Discrepancy: The solar wind speed predicted near the Earth using the present scheme involving the inverse correlation between FTE and SWS does not always agree with the observed values. The agreement between the two is very good at times and at certain other times the discrepancy is inexplicably high. In our present study, we found that the correlation between FTE, obtained using the daily values of solar wind speed for inverse mapping (V in Eq. 1) and $N_{max} = 22$, and

SWS near the Earth, is not consistently high at all times. This inconsistency can be expalined on the basis of solar wind speed profiles near the Sun and Earth, types of interaction between fast and slow streams in the heliosphere and distribution of coronal magnetic field on the source surface obtained using PFSS model.

There are two types of stream–stream interaction. In Type I, a high speed stream flows ahead of a low speed stream and a rarefaction region is formed between them, giving rise to a speed profile at 1 AU with speed gradually changing from high to low. On the other hand, when a low speed stream is flowing ahead of a high speed stream, a compression region or an interaction region is formed at the interface between the streams. This is Type II interaction.

Observations of photospheric magnetic field show that the field within coronal holes varies smoothly from centre to boundary whereas the magnetic field on the source surace computed using PFSS model varies significantly from one point to the other, especially near the boundaries of open field regions or near magnetic neutral lines. Therefore, FTE, computed using Eq. 2, is determined by the source surface magnetic field. The distribution of computed FTE from center to boundary of the hole coincidentally matches with the speed profile including a rarefaction region (Type I) if the solar wind from hole's center is ahead of that from the hole's boundary. On the other hand, if the solar wind from hole's center is behind that from hole's boundary, the FTE distribution will not match the speed profile including an interaction region (Type II). It is very likely that the correlation between SWS and FTE is highest when the speed profile is created by Type I interaction. Consequently, the predicted value matches best with the observed value, though it does not represent the causal relationship between FTE and SWS. On the other hand, when the speed profile near the Earth is formed by Type II interaction, the correlation is low and the prediction fails.

It should be noted that the solar wind speed profile obtained at 1 AU is the result of the interaction between solar winds of different speeds as they propagate outwards and includes both Type I and Type II interactions. And, we know that the interaction is stronger at larger distances from the Sun. Therefore, speed profile near the Earth must be significantly different from that near the Sun. In fact, the solar wind profile obtained at 0.31 AU by Helios in 1974 exhibited only two levels with high and low speed streams separated by a sharp gradient (Schwenn, 1990). Moreover, solar wind speed detected by Ulysses near solar minimum at latitudes above 30°, a region where all the solar wind is believed to originate from coronal holes, is nearly constant (Phillips, 1995). Therefore, if at all there exists a relationship between FTE and solar wind speed, FTE computed at the source surface must correlate with the solar wind speed near the Sun, where the effect of stream interaction can be neglected.

HCCSSS Model: The radial component of the heliospheric magnetic field (HMF), as detected by Ulysses, is latitude-independent (Smith and Balogh, 1995), and can be taken as uniform on a spherical surface above $\sim 5\ R_\odot$ (Suess and Smith, 1996; Suess et al., 1996). The magnetic field distribution on the source surface obtained using the PFSS model does not agree with this observation. This implies

that the FTE calculated using PFSS model lacks physical foundation even near the Sun and, the relationship established between FTE and SWS is questionable.

Owing to the uniform distribution of the HMF, FTE will be determined by the field strength in coronal holes on the photosphere, rather than the source surface field. The horizontal current–current sheet–source surface (HCCSSS) model (Zhao and Hoeksema, 1995; Zhao, Hoeksema and Rich, 2002) yields uniform magnetic field on the source surface, located at 15 $R_{\odot}$. Preliminary results using HCCSSS model show that the computed FTE (anti)correlates poorly with the observed solar wind speed near the Earth. In order to see if there exists any relationship between FTE and SWS near the Alfvén critical point, we plan to use the FTE computed using the HCCSSS model and the solar wind speed measured by Helios near 0.3 AU and Ulysses at higher latitudes. The analysis will be simpler since there is little interaction between fast and slow winds in these data sets. If there exists a relation, we plan to map the predicted speed near the Sun to 1 AU using a time–dependent full 3-D MHD code (Hayashi et al., 2003) simulating the interaction between solar wind streams with different speed.

In the wake of the above discussion we would emphasize that the FTE, used in the prdiction of the solar wind speed near the Earth, is obtained based on a model which has arbitrary dependence on parameters such as the number of spherical harmonics or on the method of inverse mapping. In addition, the correlation coefficient between the FTE and SWS near the Earth is usually less than 0.5. Moreover, a wide body of observations show that slow solar wind originate from regions surrounding the coronal holes. Also, the composition of slow solar wind is distinctly different from the fast solar wind and is identical to large coronal loops well separated from coronal holes. Therefore, at this juncture, it is necessary to think of alternate ways of correlating the SWS to the coronal magnetic field.

Acknowledgements:

This work is supported by the National Aeronauticas and Space Administration grant NAG5-9784, National Science Foundation grant NSF 00-67, MURI grants SA3206 and F005001. One of the authors (BP) wishes to thank Dr. Y-M. Wang, National Naval Research Laboratory, for the many discussions that helped this work. The authors also wish to thank the referees for their valuable comments and suggestions.

5 References

Arge, C.N., and Pizzo, V. J., Improvement in the prediction of solar wind conditions using near–real time solar magnetic field updates, *Journal Geophys. Res.,* **105**, 10465-10479, 2000.

Bala, B., Synoptic maps of solar wind: comparison of IPS data and the NOAA/SEC version of the Wang and Sheeley model, *Solar Phys.,* **195**, 195–208, 2000.

Crooker, N. U., A. J. Lazarus, J. L. Phillips, J. T. Steinberg, A. Szabo, R. P. Lepping and E. J. Smith, Coronal streamer belt asymmetries and seasonal solar wind variations deduced from Wind and Ulysses data, *Journal Geophys. Res.,* **102**, 4673–4679, 1997.

Hoeksema, J. T., Structure and evolution of the large scale solar and heliospheric magnetic fields, Ph. D. Thesis, 1984.

Hayashi, K., M. Kojima, M. Tokumaru and K. Fujiki, MHD tomography using interplanetary scintillation measurement, *Journal Geophys. Res.,* **108**, doi:10.1029/2002JA009567, 2002.

Hakamada K. and M. Kojima, Solar wind speed and expansion rate of the coronal magnetic field during Carrington rotation 1909, *Solar Phys.,* **187**, 115–122, 1999.

Hakamada, K., M. Kojima, M. Tokumaru, T. Ohmi, A. Yokobe, and K. Fujiki, Solar wind speed and expansion rate of the coronal magnetic field in solar maximum and minimum phases, *Solar Phys.,* **207**, 173–185, 2002.

Levine, R. H., Altschuler, M.D. and Harvey, J. W., Solar sources of the interplanetary magnetic field and solar wind, *Journal Geophys. Res.,* **82**, 1061–1065, 1977.

Neugebauer, M., P. C. Liewer, E. J. Smith, R. M. Skoug and T. H. Zurbuchen, Sources of the solar wind at solar activity maximum, *Journal Geophys. Res.,* **107**, 1488, doi:10.1029/2001JA000306, 2002.

Phillips, J. L., S. J. Bame, A. Barnes, B. L. Barraclough, W. C. Feldman, B. E. Goldstein, J. T. Gosling, G. W. Hoogeveen, D. J. McComas, M. Neugebauer and S. T. Suess, Ulysses solar wind plasma observations from pole to pole, *Geophys. Res. Lett.,* **22**, 3301–3304, 1995.

Schwenn, R. Large–scale structure of the interplanetary medium, in Physics of the inner heliosphere 1 Large–scale phenomena, R. Schwenn and E. Marsch (eds.), Springer–Verlag, 99–181, 1990.

Smith, E. J. and A. Balogh, Ulysses observations of the radial magnetic field, *Geophys. Res. Lett.,* **22**, 3317–3320, 1995.

Suess, S. T. and E. J. Smith, Latitudinal dependence of the radial IMF component – coronal imprint, *Geophys. Res. Lett.,* **23**, 3267–3270, 1996.

Suess, S. T., E. J. Smith, J. Phillips, B. E. Goldstein, S. Nerney, Latitudinal dependence of the radial IMF component - interplanetary imprint, *Astron. Astrophys.,* **316**, 304–312, 1996.

Wang, Y.-M., Empirical relationship between the magnetic field and the mass and energy flux in the source region of the solar wind, *Astrophys. J.,* **449**, L157–L160, 1995.

Wang, Y.-M., 2004, Private communication.

Wang, Y.-M., and N. R. Sheeley, Jr., Solar wind speed and coronal flux tube expansion, *Astrophys. J.,* **355**, 726–732, 1990.

Wang, Y.-M., and N. R. Sheeley, Jr., On potential field models of the solar corona, *Astrophys. J.,* **392**, 310–319, 1992.

Wang, Y.-M., and N. R. Sheeley, Jr., Global evolution of interplanetary sector structure, coronal holes, and solar wind streams during 1976–1993: Stackplot displays based on solar magnetic observations, *Journal Geophys. Res.,* **99**, 6597–6608, 1994.

Wang, Y.-M., and N. R. Sheeley, Jr., Sunspot activity and the long-term variation of the Sun's open magnetic flux, *Journal Geophys. Res.,* **107**, 1302, doi:10.1029/2001JA000500, 2002.

Wang, Y.-M., N. R. Sheeley, Jr., J. L. Phillips, B. E. Goldstein, Solar wind stream interactions and the wind speed–expansion factor relaionship, *Astrophys. J.,* **488**, L51–L54, 1997.

Zhao , X.-P., and J. T. Hoeksema, Prediction of interplanetary magnetic field strength, *Journal Geophys. Res.,* **100**, 19–33, 1995.

Zhao, X.-P., J. T. Hoeksema and N. B. Rich, Modeling the radial variation of coronal streamer belts during sunspot ascending phase, *Advances in Space Res.,* **29**, 411–416, 2002

Figure Captions

Figure 1. Variation of θ with N_{max}

Variation of heliographic latitude θ, with N_{max}, of the foot points of open field lines at selected locations on the source surface for CR 1829. The vertical line corresponds to $N_{max} = 22$. Here, tt(Nmax) – tt(Nmax = 9) on the Y-axis is the difference of computed values of θ for different N_{max} from the reference value, $N_{max} = 9$. On top of each panel, 'wso' represents the Wilcox Solar Observatory, the input photospheric magnetic field data and the numbers in parenthesis represent the location of open field lines (θ, ϕ) on source surface selected for the study. In this figure, only those locations where tt(Nmax) - tt(Nmax = 9) is larger than $\pm 2^\circ$ were shown, hence the apparent randomness in the source surface location.

Figure 2. Variation of ϕ with N_{max}:

Same as Figure 1 but for ϕ. Here, p(Nmax) – p(nmax = 9) represent the difference in the computed values of ϕ for different N_{max} from the reference value, $N_{max} = 9$.

Figure 3. Variation of FTE with N_{max}:

Variation of FTE with N_{max} for CR 1829. FTE is calculated at locations shown in Figures 1 and 2. The vertical line corresponds to $N_{max} = 22$.

Figure 4. Reconstructed photospheric synoptic maps: WSO

Top left panel: The observed photospheric magnetic field for CR 1763 from Wilcox Solar Observatory. The remaining panels are the photospheric magnetic fields reconstructed using PFSS model with different N_{max}.

Figure 5. Reconstructed photospheric synoptic maps: KPK

Same as Figure 4 but for Kitt Peak data.

Figure 6. Optimum N_{max}: WSO data

The optimum N_{max}, for which correlation between the observed and the reconstructed photospheric magnetic fields is the highest, for different Carrington rotations and for WSO data.

Figure 7. Optimum N_{max}: KPK data

Same as Figure 6 but for Kitt Peak data.

Figure 8. Correlation coefficient and inverse mapping

Correlation coefficient, between SWS and $\log_10$(FTE), for different mapping back method (transit times or V in Eq. 1) and different phases of solar cycle. On the X-axis, 1.0 represents daily values of solar wind observed at 1 AU, 27.0 is the 27 day running average of observed solar wind, and, 4.5, 4.0

and 5.0 are the approximate solar wind transit times in the *constant speed approximation* used by different authors.

Figure 9. Scatter plot: 1992–1997

Scatter plot of SWS *vs* FTE during 1992–1997. For the inverse mapping, the observed daily values of solar wind speed have been used (denoted by 'mapback: 1.0' in the plot). A correlation coefficient of -0.42 was obtained. This is the highest during the entire period of study.

Figure 10. Scatter plot: 1982–1987

Same as Figure 10 but for 1982–1987. Correlation coefficient is -0.29, which is the lowest obtained during the period of study.

Figure 11. Inverse mapping and solar longitudes

The range of longitudes of solar wind sources in the inner corona when mapped back from 1 AU using different inverse mapping method, ie., solar wind speed in Eq. 1. On the X-axis, 'sws' represents the daily values of solar wind speed, 5.0, 4.5 and 4.0 are different transit times in the *constant speed approximation*. 27 represents the 27-day running average of the observed daily values. On the Y-axis, the longitudes in degrees are marked. The longitudes are obtained using Eq. 1. assuming an initial longitude of 0°.

Figure 12. Inverse mapping: histogram of shifts in ϕ

Histogram of shifts, in degrees, in longitude of the coronal sources of solar wind caused by different mapping back techniques. The shifts are obtained as a difference from the longitude obtained using the daily values of solar wind speed. On each panel the phase of solar cycle and the total number of data are marked.

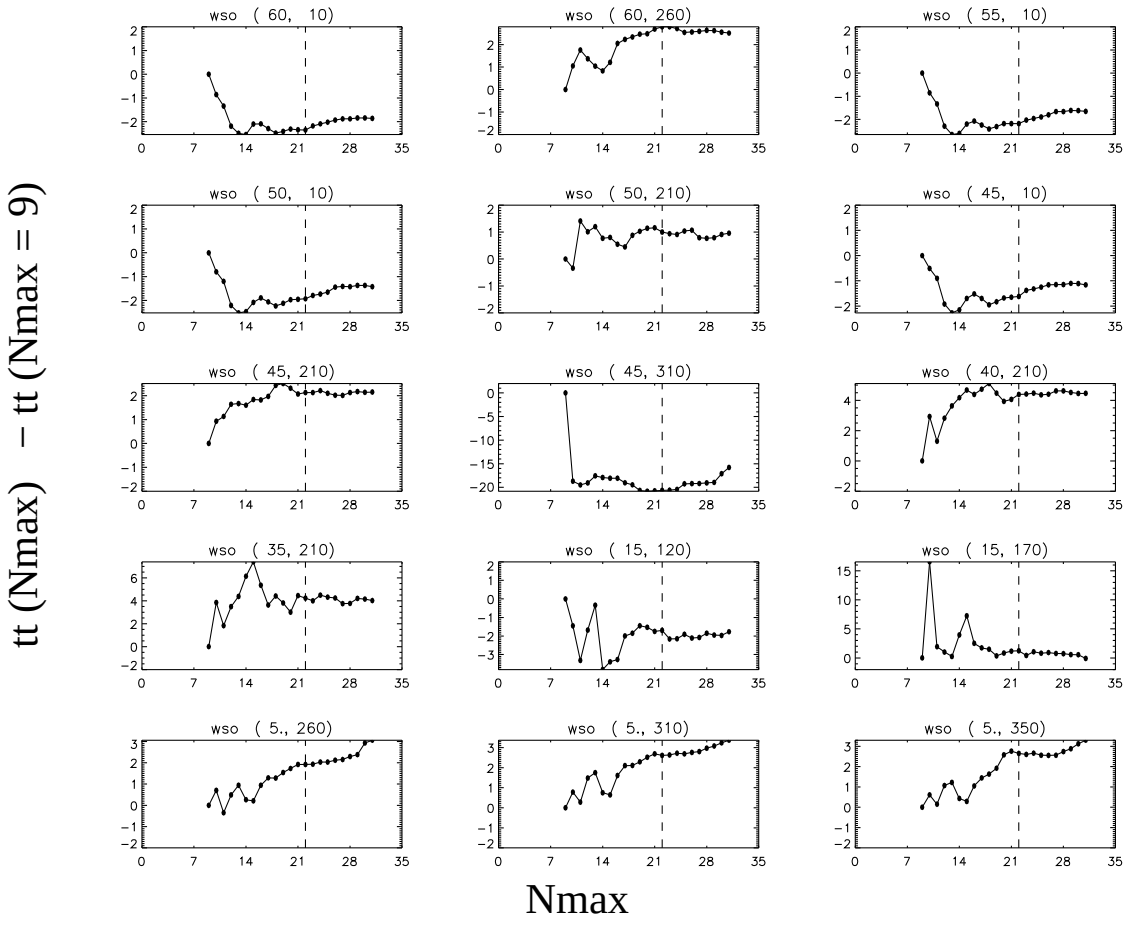

Figure 1: Variation of heliographic latitude θ, with N_{max}, of the foot points of open field lines at selected locations on the source surface for CR 1829. The vertical line corresponds to $N_{max} = 22$. Here, tt(Nmax) – tt(Nmax = 9) on the Y-axis is the difference of computed values of θ for different N_{max} from the reference value, $N_{max} = 9$. On top of each panel, 'wso' represents the Wilcox Solar Observatory, the input photospheric magnetic field data and the numbers in parenthesis represent the location of open field lines (θ, ϕ) on source surface selected for the study. In this figure, only those locations where tt(Nmax) - tt(Nmax = 9) is larger than $\pm 2^\circ$ were shown, hence the apparent randomness in the source surface location.

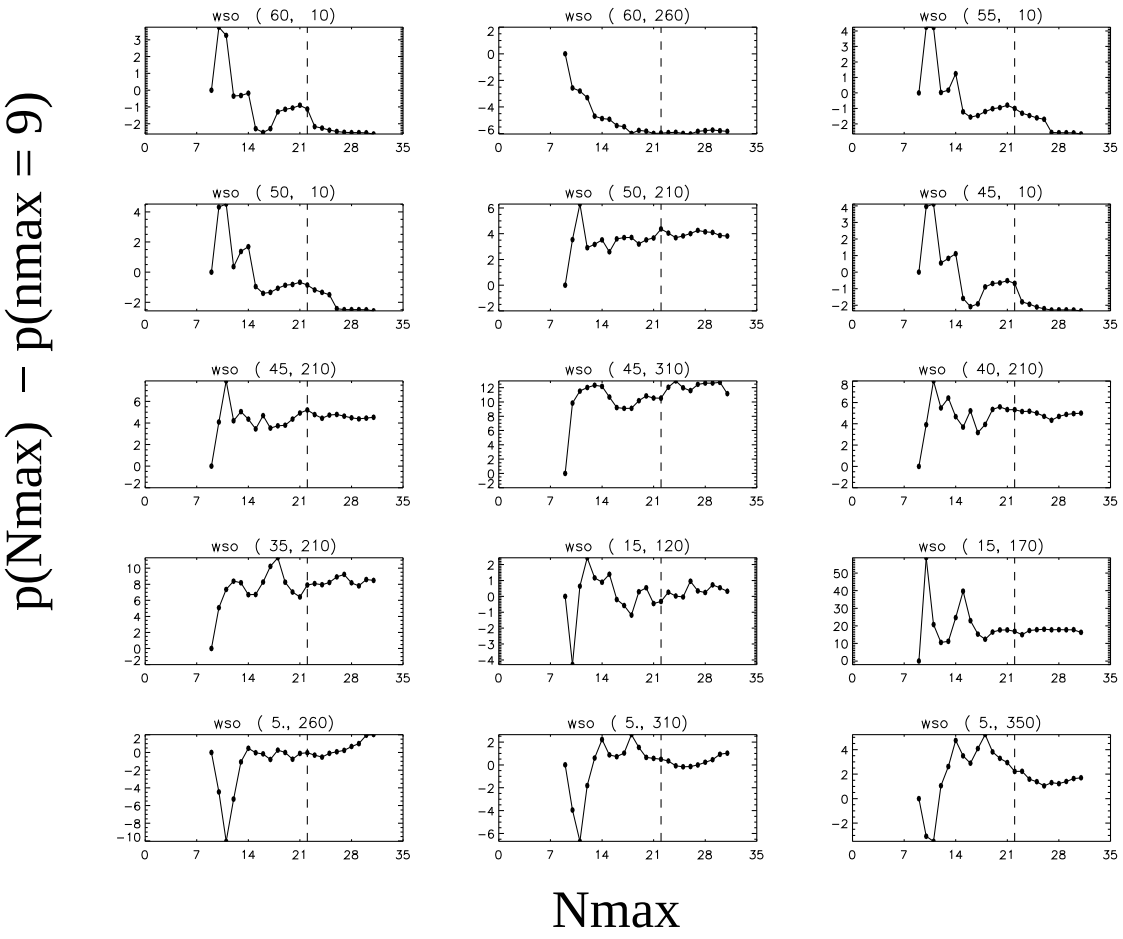

Figure 2: Same as Figure 1 but for ϕ. Here, p(Nmax) – p(nmax = 9) represent the difference in the computed values of ϕ for different N_{max} from the reference value, $N_{max} = 9$.

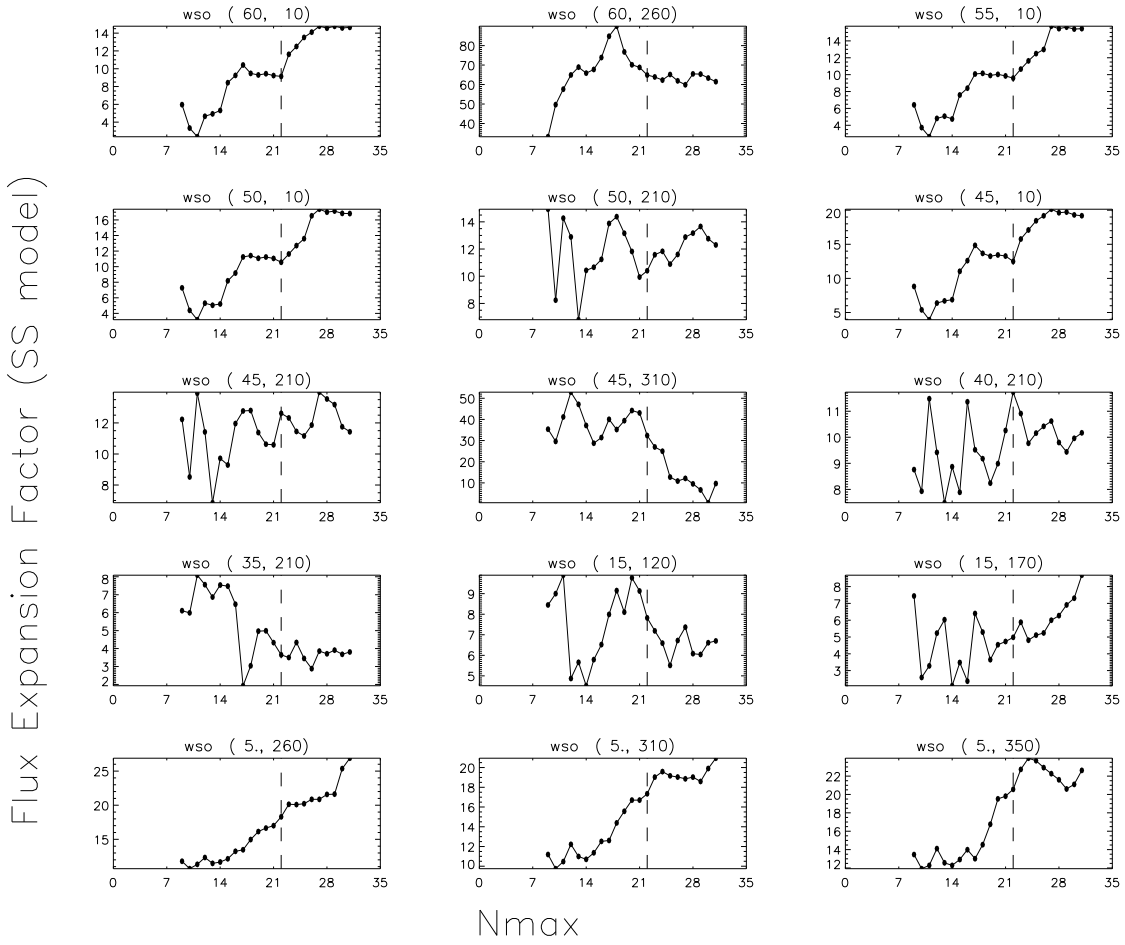

Figure 3: Variation of FTE with N_{max} for CR 1829. FTE is calculated at locations shown in Figures 1 and 2. The vertical line corresponds to $N_{max} = 22$.

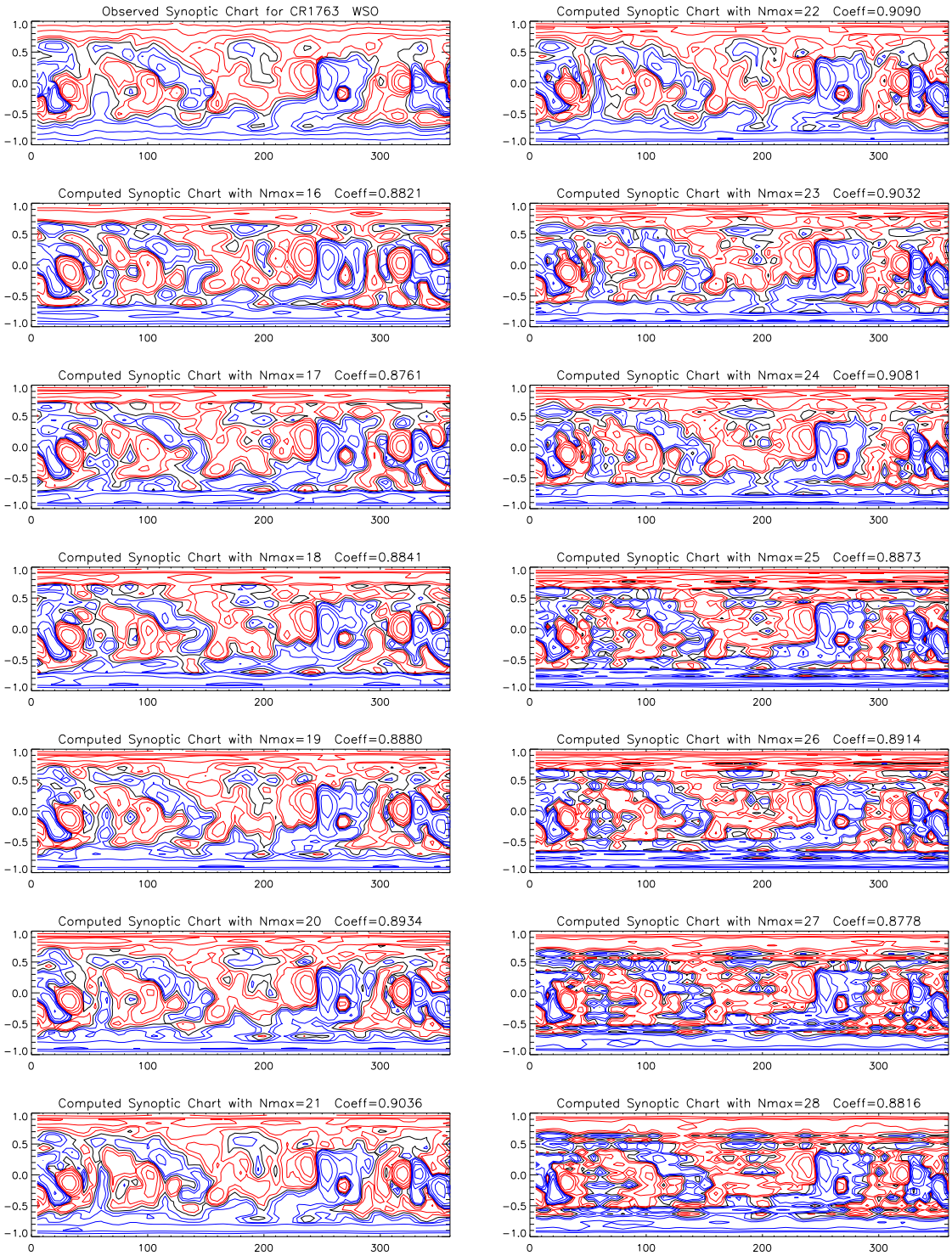

Figure 4: Top left panel: The observed photospheric magnetic field for CR 1763 from Wilcox Solar Observatory. The remaining panels are the photospheric magnetic fields reconstructed using PFSS model with different N_{max}.

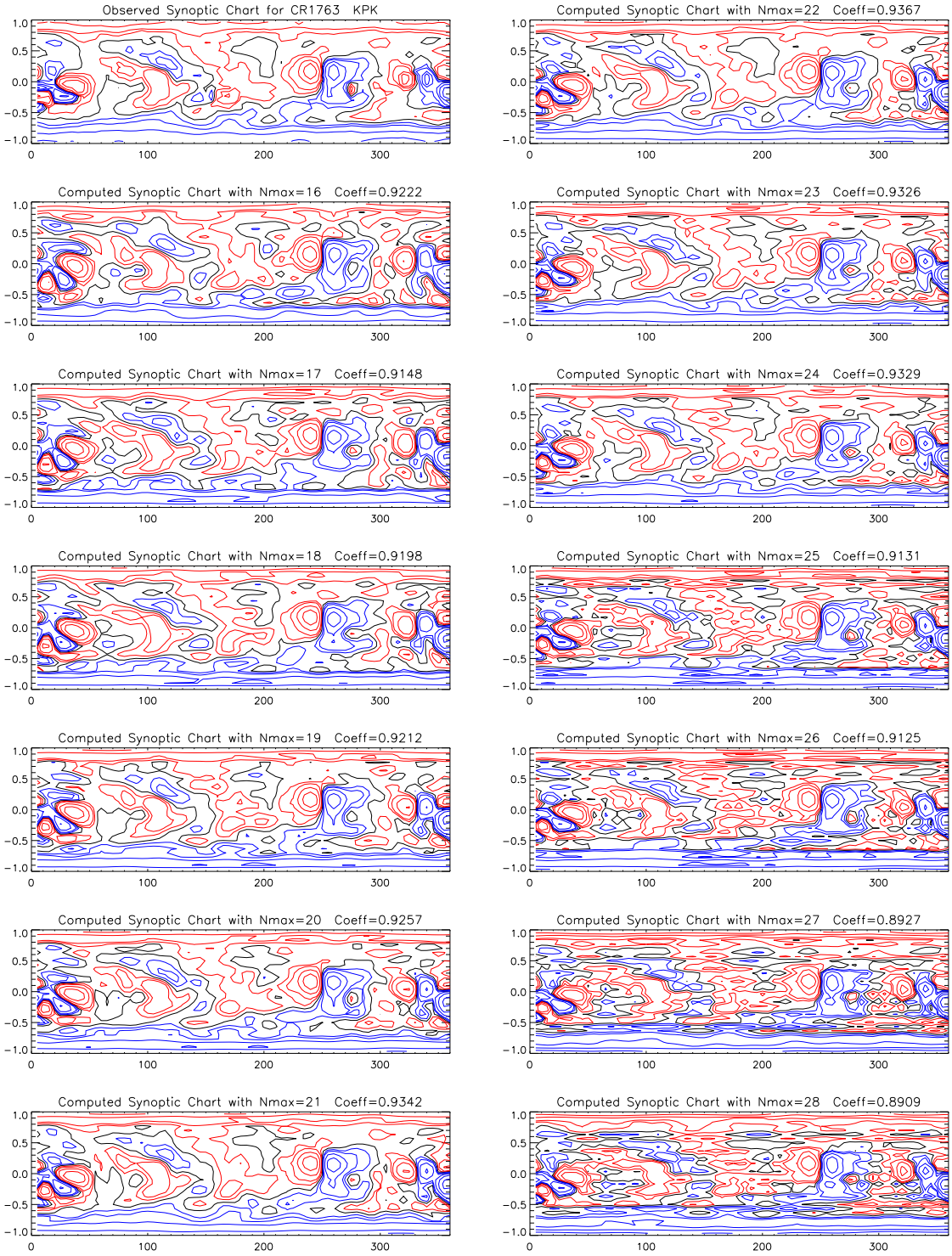

Figure 5: Same as Figure 4 but for Kitt Peak data.

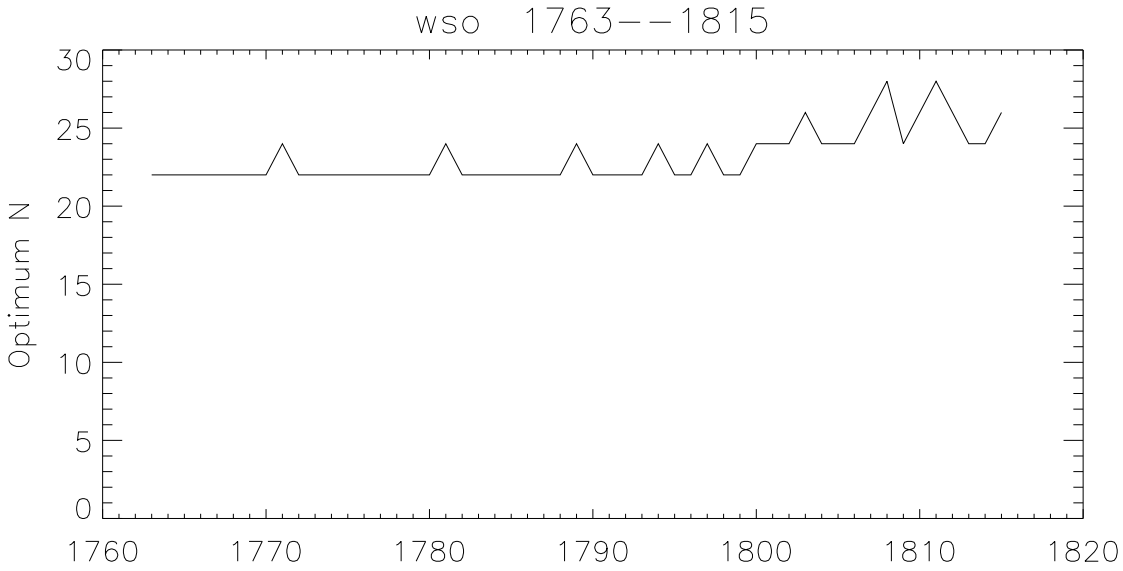

Figure 6: The optimum N_{max}, for which correlation between the observed and the reconstructed photospheric magnetic fields is the highest, for different Carrington rotations and for WSO data.

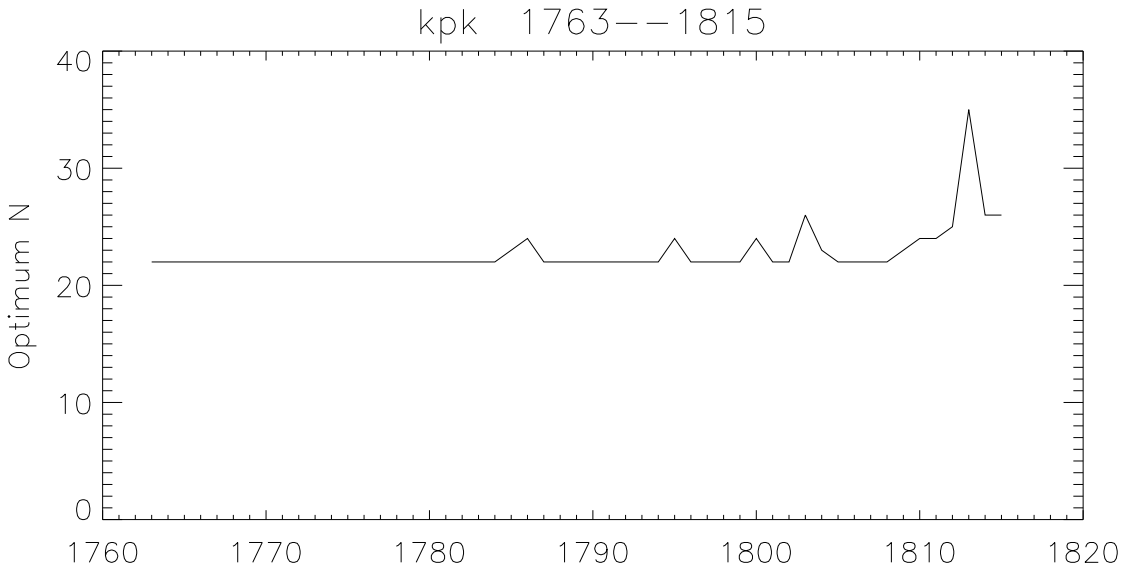

Figure 7: Same as Figure 6 but for Kitt Peak data.

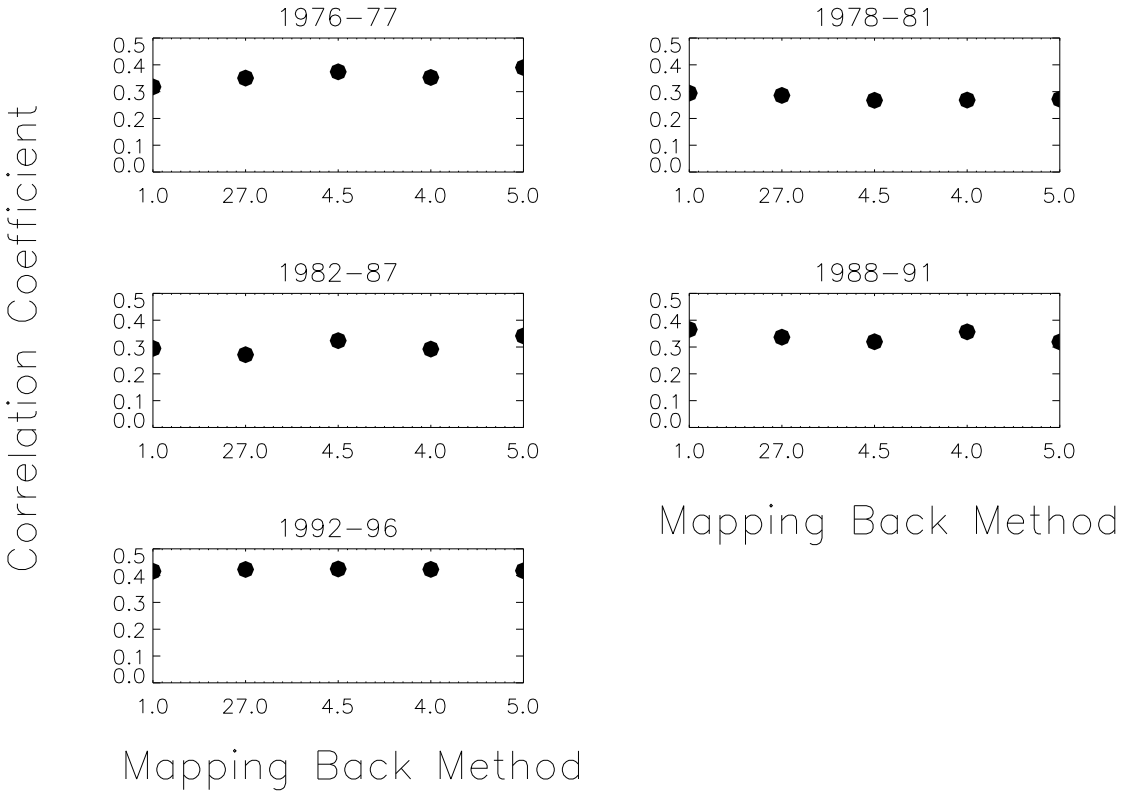

Figure 8: Correlation coefficient, between SWS and $\log_1 0$(FTE), for different mapping back method (transit times or V in Eq. 1) and different phases of solar cycle. On the X-axis, 1.0 represents daily values of solar wind observed at 1 AU, 27.0 is the 27 day running average of observed solar wind, and, 4.5, 4.0 and 5.0 are the approximate solar wind transit times in the *constant speed approximation* used by different authors.

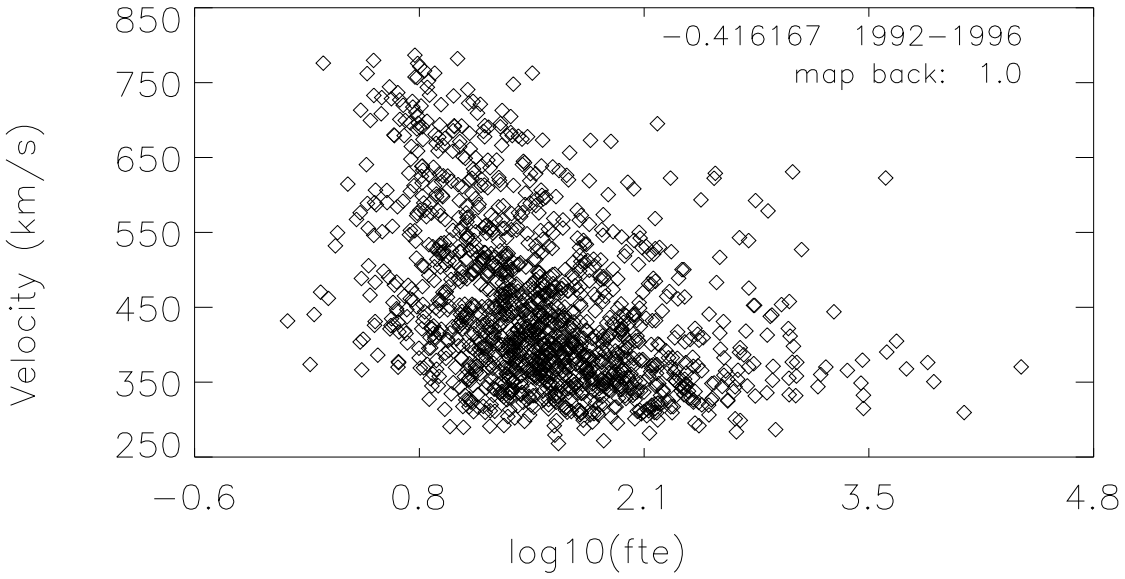

Figure 9: Scatter plot of SWS *vs* FTE during 1992–1997. For the inverse mapping, the observed daily values of solar wind speed have been used (denoted by 'mapback: 1.0' in the plot). A correlation coefficient of -0.42 was obtained. This is the highest during the entire period of study.

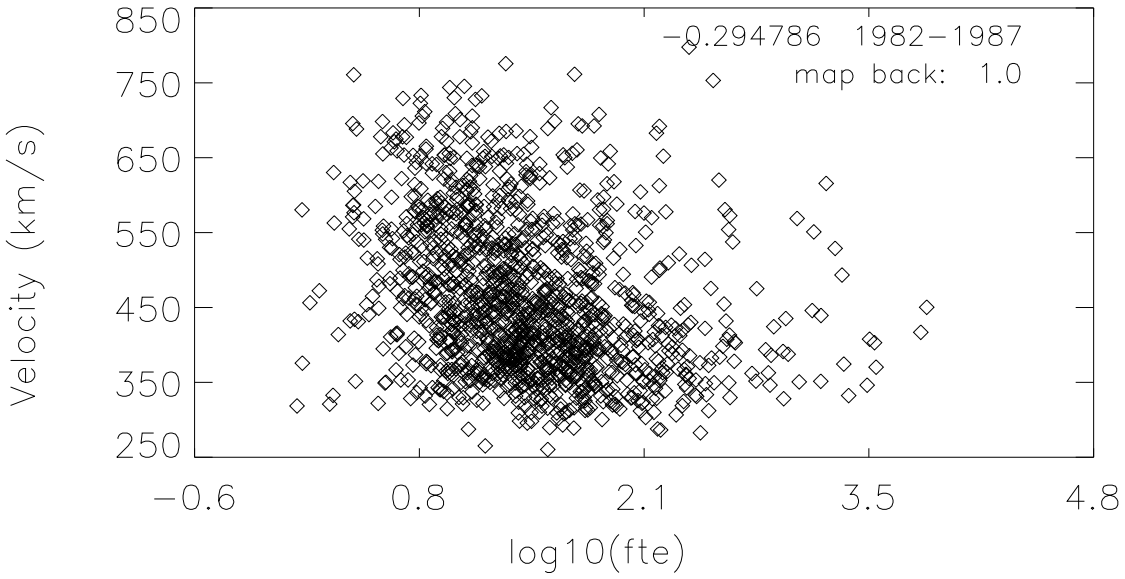

Figure 10: Same as Figure 10 but for 1982–1987. Correlation coefficient is -0.29, which is the lowest obtained during the period of study.

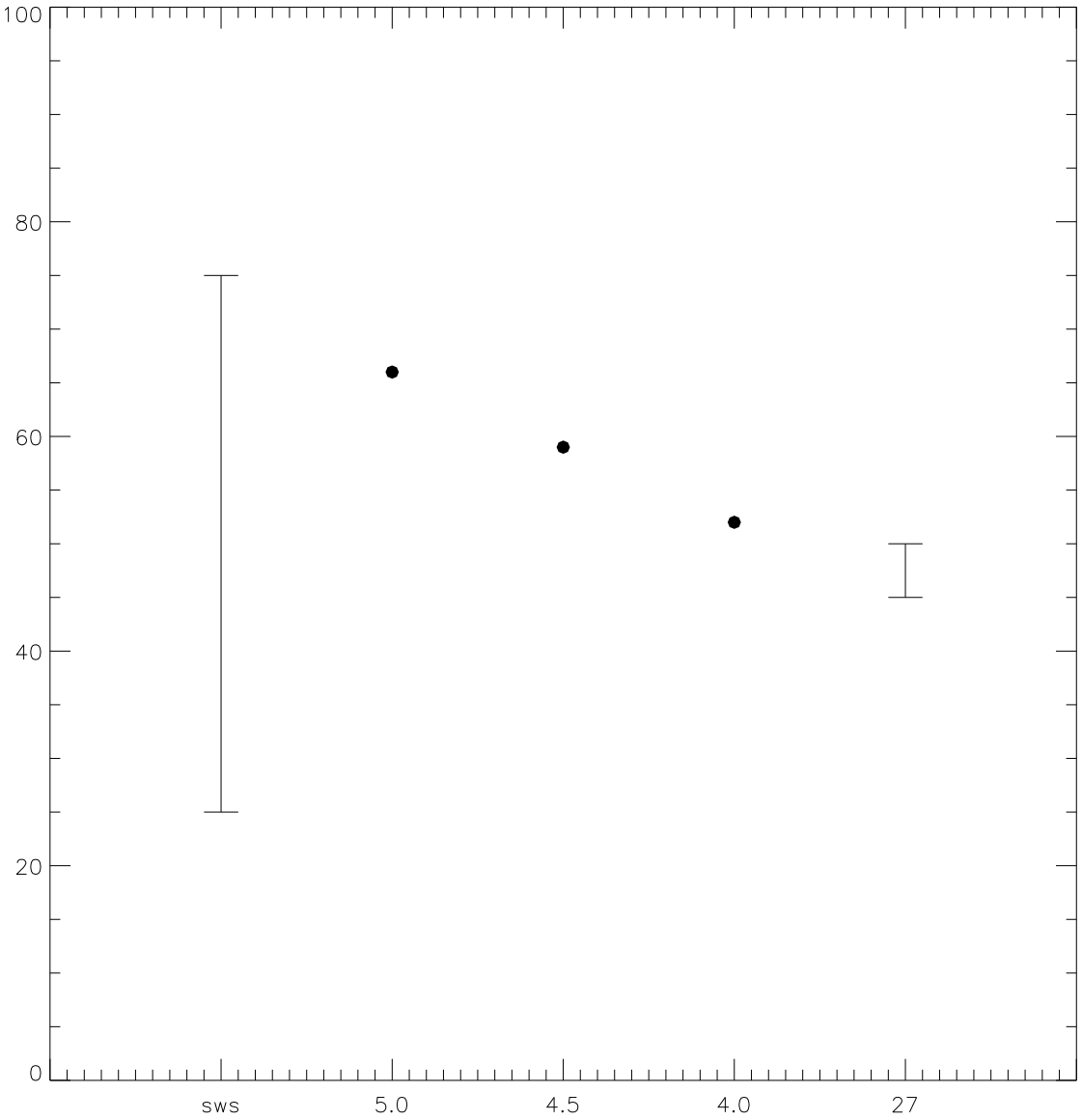

Figure 11: The range of longitudes of solar wind sources in the inner corona when mapped back from 1 AU using different inverse mapping method, ie., solar wind speed in Eq. 1. On the X-axis, 'sws' represents the daily values of solar wind speed, 5.0, 4.5 and 4.0 are different transit times in the *constant speed approximation*. 27 represents the 27-day running average of the observed daily values. On the Y-axis, the longitudes in degrees are marked. The longitudes are obtained using Eq. 1. assuming an initial longitude of 0°.

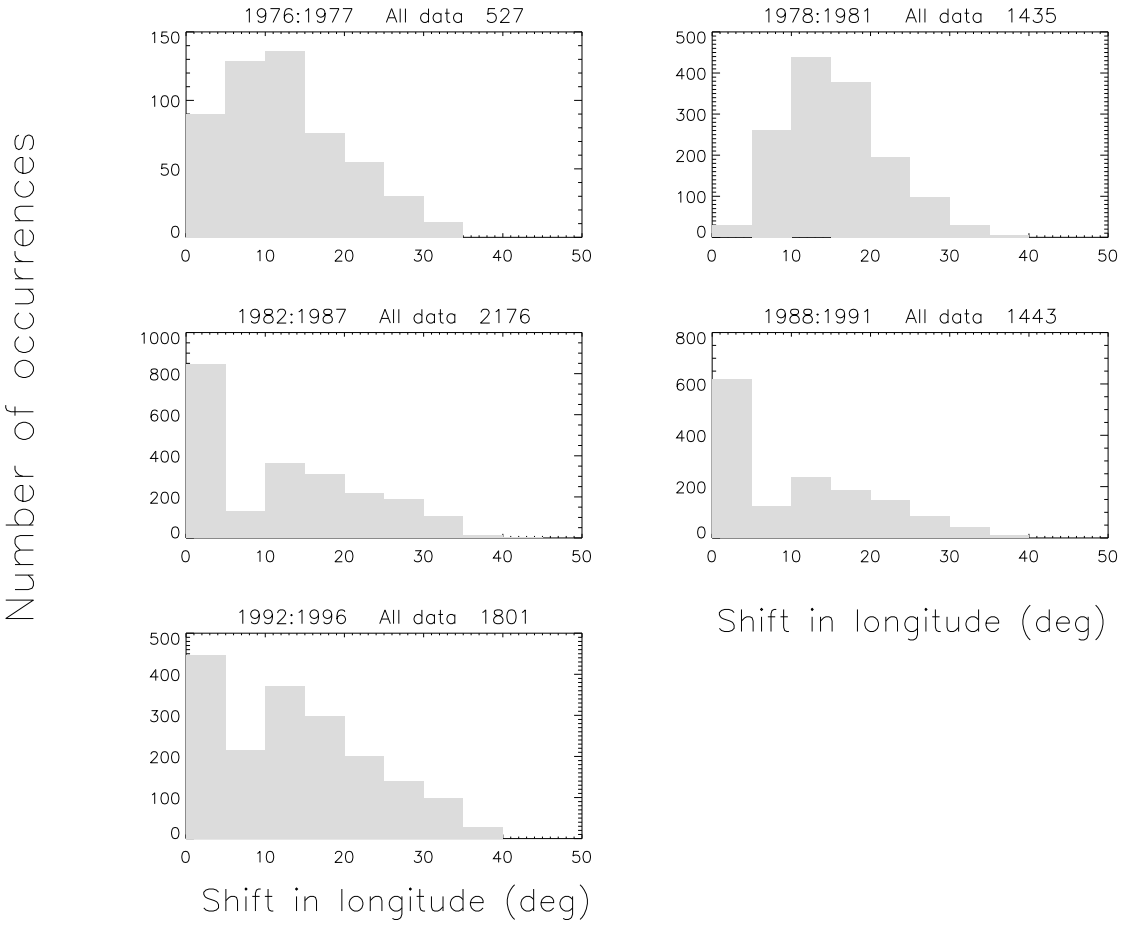

Figure 12: Histogram of shifts, in degrees, in longitude of the coronal sources of solar wind caused by different mapping back techniques. The shifts are obtained as a difference from the longitude obtained using the daily values of solar wind speed. On each panel the phase of solar cycle and the total number of data are marked.